Pure Appl. Geophys. 173 (2016), 3273–3290

DOI 10.1007/s00024-015-1161-3

Pure and Applied Geophysics

Analysis of the Aeromagnetic Anomalies of the Auca Mahuida Volcano, Patagonia, Argentina

L. M. Longo,[1,2] R. De Ritis,[3] G. Ventura,[3,4] and M. Chiappini[3]

Abstract—We present the analysis of the subsurface structure of the Auca Mahuida volcano based on high-resolution aeromagnetic data integrated with the available geological information. Most of the detected magnetic anomalies have a dipolar structure opposite to that of the present geomagnetic field. According to the available geochronological data and paleomagnetic measurements, the source bodies of Auca Mahuida mainly emplaced in the Matuyama reverse polarity chron. The Reduction-to-the-Pole map confirms that the magnetization direction is mainly reverse with only few anomalies normally magnetized. Two opposite, coexisting polarities do not allow to fully remove the dipolar character of the field in the Reduction-to-the-Pole transformation. Therefore, we model the measured anomaly field by applying analytical techniques that are independent of the magnetization direction. The obtained anomaly strikes and source geometries indicate an emplacement of intrusive bodies controlled by the regional faults affecting the Auca Mahuida basement and the sedimentary successions of the Neuquén basin. Magma upraised along these faults and fractures feeding the volcanic activity and subsequently crystallized. The averaged power spectrum and Euler Deconvolution indicate source depths consistent with those of the intrusions recognized in wells. Borehole data highlight the widespread presence of intrusive bodies below the Auca Mahuida central crater and the peripheral sectors at depth of 2 km below sea level. These bodies have played a major role in the thermal maturation of hydrocarbons and in the subsequent accumulation of oil below the volcano. The obtained results shed light on the Auca Mahuida feeding system and on the intrusions geometry, also pointing out the effectiveness of the magnetic prospecting in the oil industry even in presence of strong remanent magnetization.

Key words: Magnetic anomalies, aeromagnetic data, oil fields and volcanoes, reverse polarity, Auca Mahuida volcano.

1. Introduction

Magnetic anomalies constitute a powerful tool to obtain information about the subsurface when magnetic susceptibility contrasts are present (Finn *et al.* 2001; Blanco-Montenegro *et al.* 2006); this is especially true when igneous rocks intrude sedimentary basins. From the magnetic point of view, sediments are mostly transparent (Reynolds 2011). Thus, structures such as magmatic dikes, sub-circular conduits, and sills emplaced within sedimentary sequences are likely sources of intense magnetic anomalies because of their high susceptibility contrast. Many studies of magnetic anomalies in volcanoes have demonstrated the usefulness of this type of data for the characterization of the subsurface (Blanco 2003; De Ritis *et al.* 2005).

The Auca Mahuida (hereafter AM) volcano is located in the north eastern sector of the Neuquén basin in Argentina (Fig. 1). A high-resolution aeromagnetic survey was conducted for YPF S.A. in the central AM area in 2001. The survey was designed to supplement the information provided by the seismic prospection, which does not cover the central crater area due to its rough topography.

Magnetic modeling has furnished a reliable image of the intrusive bodies inside the sedimentary rocks, their depth intervals and magnetization. Mostly, the sources of the magnetic anomalies emplaced in a reverse magnetic chron because they exhibit a dipolar structure opposite to that expected in the Southern hemisphere under a magnetizing Earth field with normal polarity. In fact, age determination of the AM samples show a time interval of 2.03–0.88 Ma (Bermúdez and Delpino 1998), which implies that volcanic activity concentrated during the reverse polarity Matuyama Chron. Therefore, the magnetic modeling technique adopted by us takes into account

[1] YPF, Gerencia de Geofísica, Buenos Aires, Argentina.
[2] Facultad de Ciencias Astronómicas y Geofísicas, Universidad Nacional de La Plata, La Plata, Argentina.
[3] Istituto Nazionale di Geofisica e Vulcanologia, Rome, Italy. E-mail: riccardo.deritis@ingv.it
[4] Istituto Ambiente Marino Costiero, Consiglio Nazionale delle Ricerche, Naples, Italy.

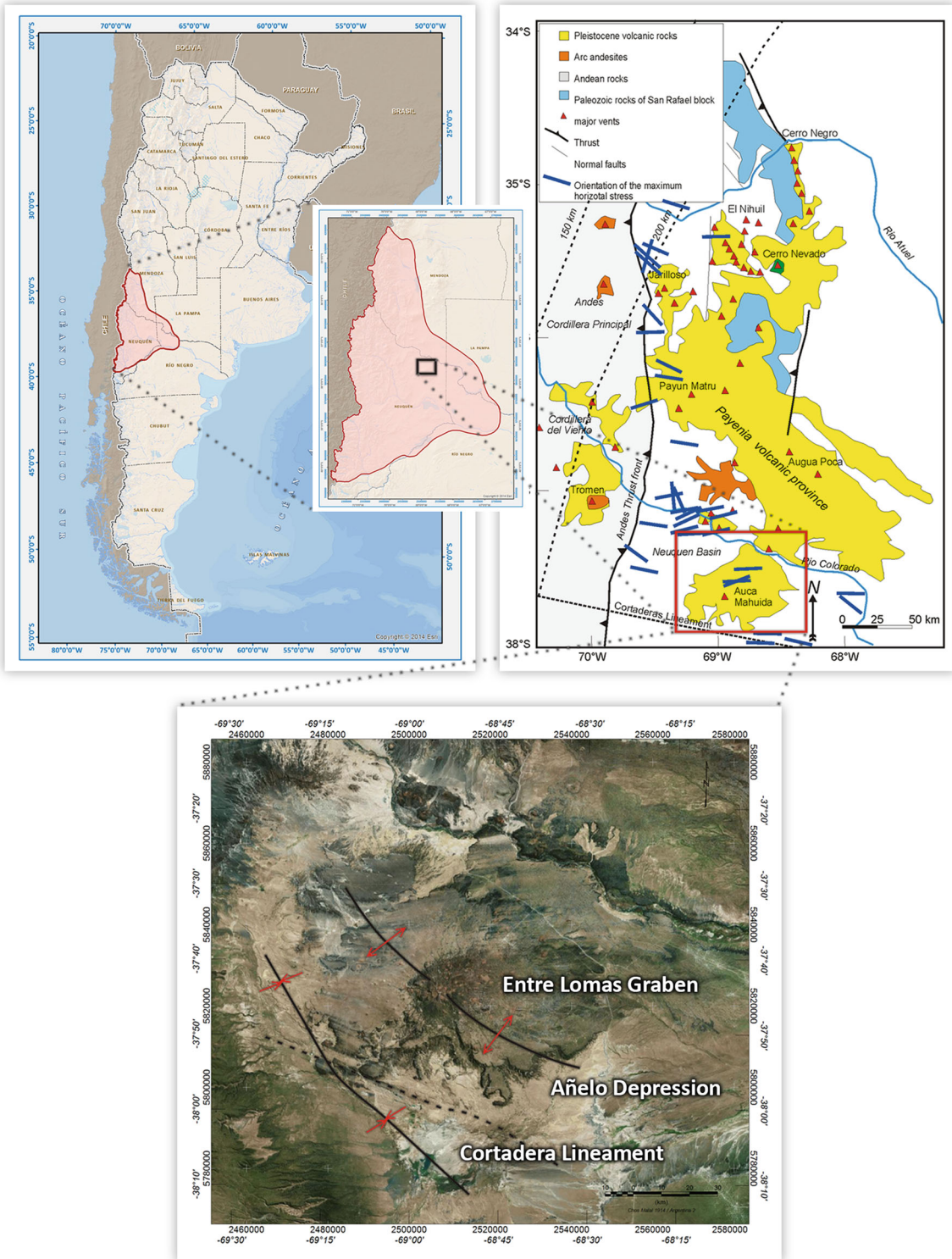

Figure 1
Top left Neuquén Basin position (*red line* inside the Argentina Republic map) together with the Auca Mahuida site within the Neuquén basin. *Top right* geological sketch map of the Payenia volcanic province. *Bottom* satellite image of the Auca Mahuida basaltic volcano complex

that the primary magnetization for the area is a strong reverse remanence. We computed the radially averaged power spectrum (Spector and Grant 1970) of the dataset, comparing the obtained depth to top of the magnetic sources with the intrusion depths measured in boreholes (Vela *et al.* 2006). Moreover, in order to obtain the 3D source geometries, we carried out the Euler Deconvolution (Thompson 1982), as well as inverse modeling (MacLeod 2013). The obtained magnetic models were interpreted using the paleomagnetic measurements, borehole data and seismic profiles as constraints, shedding light on the inner structures of the central volcano. This is a valuable result since location, geometry, and volume of igneous bodies are parameters of primary importance for the detection and evaluation of possible oil reservoirs below AM.

2. Geological Background

AM volcano is the southernmost edifice of the Payenia retroarc volcanic province, which extends in the Andean foreland between 35°and 38° S latitude (Kay and Ramos 2006; Fig. 1), and it is located about 400 km east of the outcropping front of the Andes. The volcanism started during Miocene and mainly developed between the Pliocene and the Quaternary, to the east of the roughly N–S striking Andes mountain front. The main igneous events occurred under extensional regimes that generated deep fractures, which are necessary for the uplift of the fluids from large depths. This extensional phase alternated with compressional events that built the thrust belt. The volcanism is absent to the south of the AM volcano, where the N100°E striking Cortaderas lineament, marks the southern boundary of the Miocene subduction (Kay and Ramos 2006). This boundary is marked on the surface by N100°E to E–W striking faults affecting the Añelo depression (Fig. 1). AM volcanic field lies on a NNW-SSE to NW–SE striking anticline involving the complete sedimentary sequence of the Neuquén basin (Rossello 2002; Mosquera and Ramos 2006). This sequence is affected by NNW-SSE to NW–SE striking normal faults of the Entre Lomas half-graben (Cristallini *et al.* 2006). The activity of these faults mainly developed from the Late Jurassic to Upper Cretaceous periods, with minor activity in more recent times. The approximately 6 km thick stratigraphic sequence (Fig. 2) in the AM area includes a series of deposits with ages from the Upper Triassic to Lower Tertiary. These deposits were intruded by magma between 25 and 0.5 Myr ago (Pángaro *et al.* 2004). The basement is constituted by the Choiyoi group consisting of volcanoclastic Permo-Triassic rocks: pyroclastics, intrusive, and ignimbrites (Sigismondi and Ramos 2008). These were followed, in the rift phase, by the volcanoclastic and epiclastic rocks of the Pre-Cuyo formation. AM edifice is located at 37°44′S, 68°55′W and reaches an altitude of 2258 m a.s.l. (Figure 1). AM consists of an E–W elongated lava plateau with monogenic vents and a summit polygenic cone (Ventura *et al.* 2012). The lava flows cover a surface of about 2700 km^2. The thickness of the lavas is 500 m below the central crater and decreases to virtually 0 toward the periphery Rossello 2002; Longo *et al.* 2008).

The age of the AM rocks is between 2.03 ± 0.3 and 0.88 ± 0.3 Myr and the composition varies from within-plate basalts (WPB) to trachytes (Kay and Ramos 2006; Ramos and Folguera 2010).

3. Data

3.1. Aeromagnetic Survey

A high-resolution aeromagnetic survey was conducted in the AM and Señal Cerro Bayo areas in 2001 by Carson Aerogravity company (Carson Aerogravity 2001). Magnetic data were measured by a Geometrics high sensitivity Cesium Vapor magnetometer at a sampling rate of 1 Hz, at 2830 m a.s.l. The area was surveyed using profile and tie lines oriented N–S and E–W, respectively. Line spacing was 0.5 × 0.5 km above the AM central crater and 2 × 2 km in the surrounding areas. A magnetic base station was set up in the Rincon de los Sauces airport recording the diurnal variation. The field data were diurnally corrected using the base station, the IGRF2000 model was used in order to remove the main field component, and profile and tie lines leveled in order to get as precise as possible the Total Magnetic Intensity (TMI) field (Fig. 3).

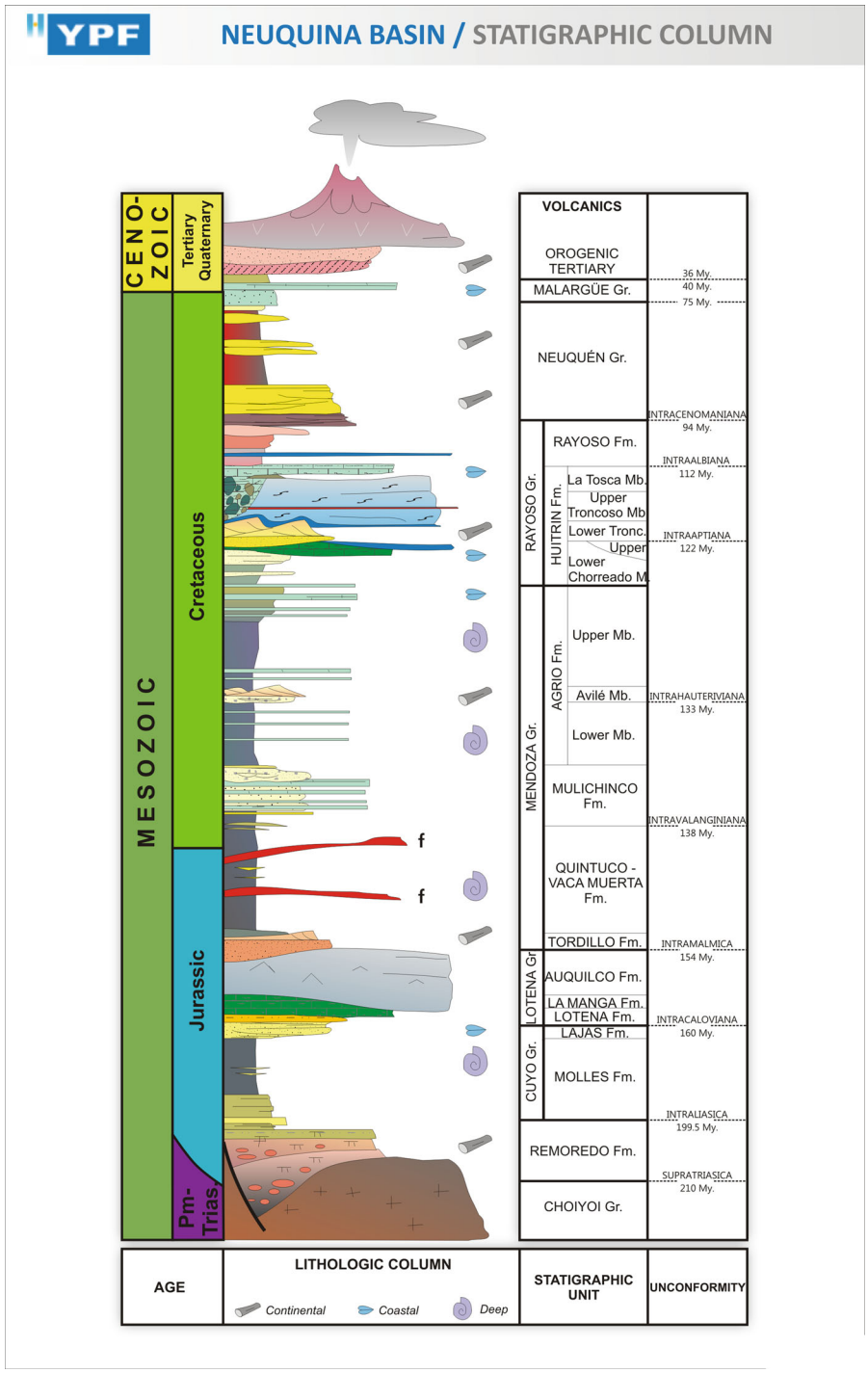

Figure 2
Stratigraphic column corresponding to the AM area. Adapted from Brisson and Veiga 1999

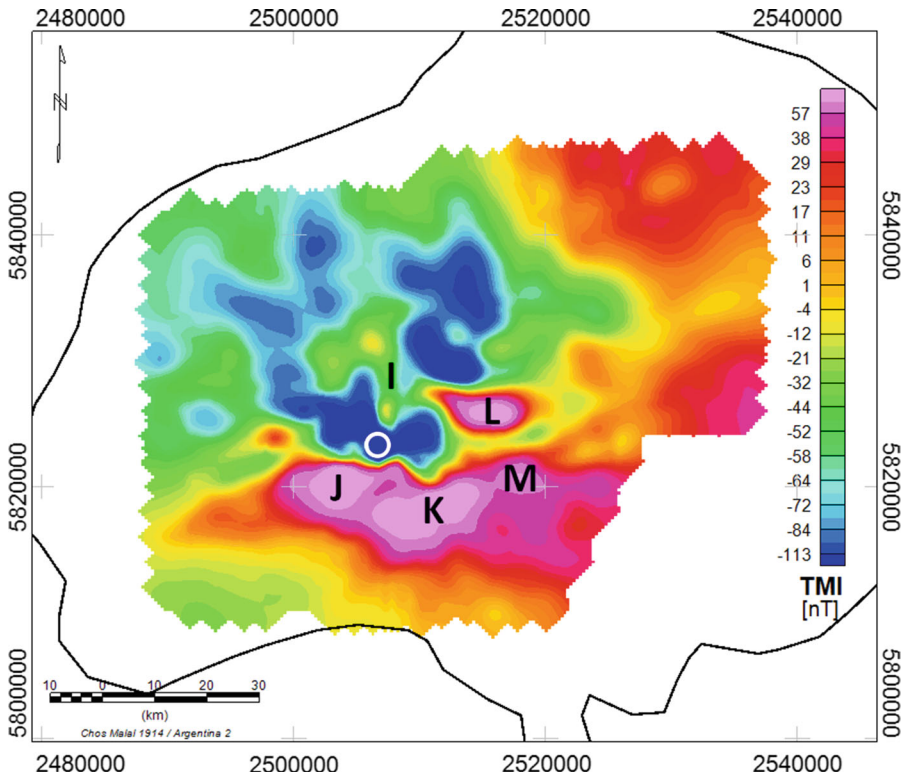

Figure 3
TMI anomaly map of the Auca Mahuida volcano. The *white circle* marks the central crater. Limit of the volcanic plateau is shown with a *black line*. The letters I, J, K, L, and M label specific anomalies discussed in the text. The aeromagnetic survey does not cover the entire plateau

3.2. *Magnetic Susceptibility Measurements and Rock Types*

Thirty-three samples were collected in the field in the AM central sector and flanks; some samples are from outcrops of the sedimentary upper Neuquén formation. The sample locations are shown in Fig. 4. The composition of the samples varies from basalts to trachytes. We measured the on-site susceptibility using a high sensitivity (1×10^{-7} SI) ZH - SM-30 magnetic susceptibility meter (Table 1; Fig. 4). The mass specific susceptibility was also determined (Table 1) in the laboratory with a Kappabridge system AGICO (KLY-2 model) on thirty samples. The measurements were carried out on the most representative lava flows, scorias and pumices of the AM area, as well as on siltstones and clays of the Neuquén formation. The measurements were carried out at the paleomagnetism laboratory of the Istituto Nazionale di Geofisica e Vulcanologia (INGV, Rome, Italy).

3.3. *Seismic and Well Data*

Seismic 2D lines and a 3D survey in time domain were available from YPF. The survey does not cover the whole AM area (Fig. 5a). Besides, the quality of the 2D lines is poor (Fig. 5 b) due to the significant thickness of surface basalts, which have a high acoustic impedance. Well data allow us to identify the formations of interest constraining the seismic section interpretation through synthetic seismograms, which provide seismic velocities. These data allow interpreting the shallower and intermediate formations, (e.g., Quintuco, Fig. 5c) at the borders of the volcanic plateau.

The depth reached by boreholes is up to 4 km below the ground level (Fig. 5), involving the

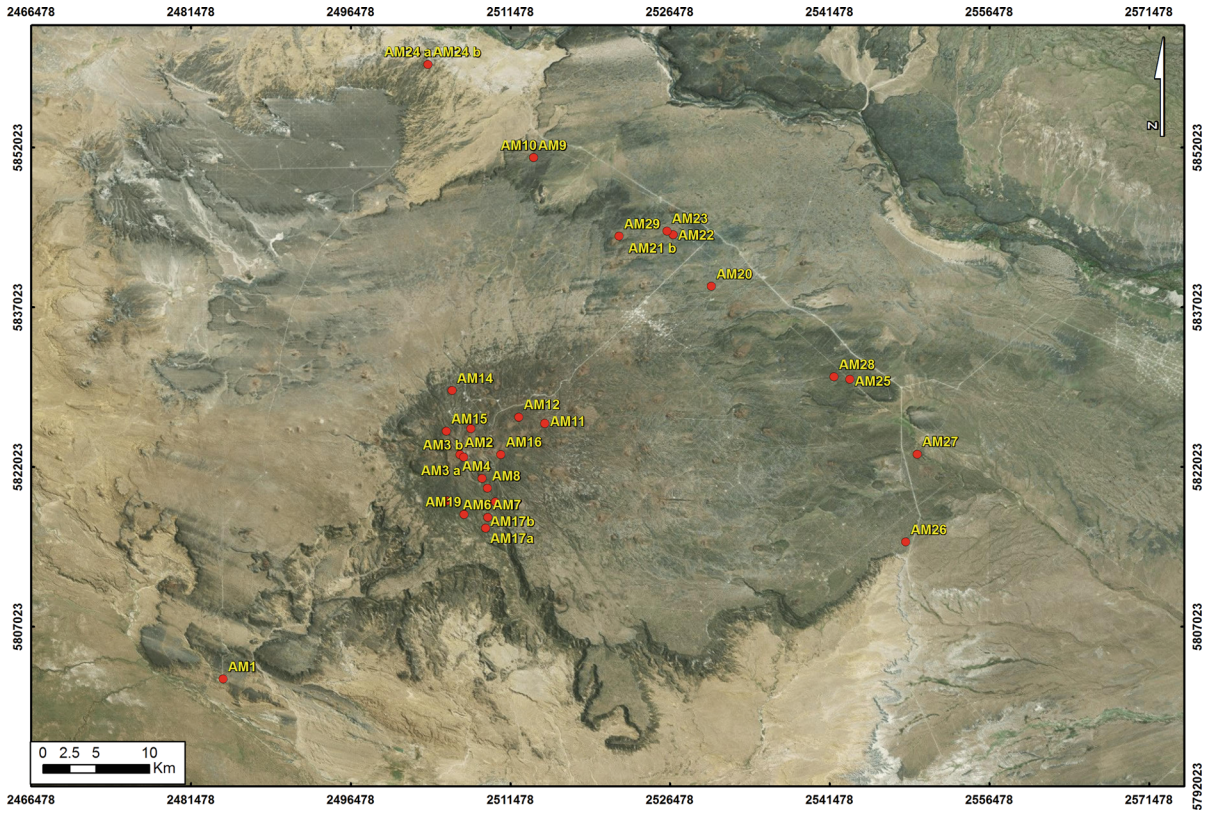

Figure 4
Location of paleomagnetic measurements on the AM complex

middle-upper parts of the sedimentary sequence. The available information includes the lithology, facies description, gamma ray, sonic and density logs (the last three are used to generate the synthetic seismograms). Moreover, samples of the sedimentary sequence and of the intrusions are available from cores of a few wells. These specimens are almost transparent and highly magnetic.

Subsurface temperature measurements were also available from the boreholes. The maximum temperature recorded at the bottom (~4 km b.s.l.) of 24 boreholes is about 180 °C, a value well below that of the Curie temperature. The depth variation of the equilibrium temperature (Fig. 6), after the usual corrections, agrees with the regional trend of the Neuquén basin (SIGISMONDI and RAMOS 2008). As a consequence, igneous rock bodies intruded into the sedimentary sequence can be magnetized and represent the source of magnetic anomalies.

4. Auca Mahuida Magnetic Anomaly Field

4.1. Topographic Effect of a Uniformly Magnetized Crustal Slab

In volcanic areas, shallow or outcropping sources (e.g., domes, cones) can be identified through their magnetic response. As a matter of fact, when a topographic magnetic effect is present, a direct correlation between topographic and magnetic features can be easily recognized (BLAKELY and GRAUCH 1983). Usually, this happens when a rough and very steep topography is present together with highly magnetized rocks. This is not the case of the AM volcano, which has a very low topographic gradient, and where such kind of correlation is not observable in the magnetic anomaly field. Nevertheless, in order to understand the possible wavelengths, amplitudes, and shape of the terrain magnetic effect, we

Table 1

Laboratory and field magnetic susceptibility measurements

Sample	*k* laboratory	*k* onsite measurementes	Lithology
AM1	0.00514	0.00837	Massive lava
AM2	0.02316	0.01366	Vesicular altered lava
AM3a	0.00346	0.02815	Massive lava
AM3b		0.02365	Massive lava
AM4	0.03302	0.01648	Massive lava
AM5	0.04029	0.02507	Massive lava
AM6	0.03839	0.01802	Massive lava
AM7	0.00506		Pumice
AM8	0.01283	0.00912	Massive lava
AM9	0.00667	0.00579	Vesicular lava close to a sedimentary dikes
AM10	0.00023	0.00009	Oxidade clay, volcaniclastic flow deposit
AM11	0.01834	0.01166	Vesicular lava close to a sedimentary dikes
AM12	0.02631	0.01400	Massive lava
AM13	0.02432	0.01933	Massive lava
AM14	0.01637	0.01314	Massive lava
AM15	0.02062	0.00911	Massive lava
AM16	0.01783	0.01077	Massive lava
AM17a	0.02071	0.01570	Massive lava
AM17b	0.01932	0.01456	Massive lava
AM18	0.02401	0.01559	Massive lava
AM19	0.02284	0.01036	Massive lava above the Neuquén sediments
AM20	0.01261	0.00752	Massive lava
AM21 a	0.01633	0.00256	Welded scoria
AM21 b		0.00089	Massive lava
AM22	0.02039		Vesicular lava
AM23	0.02535	0.01377	Massive lava
AM24 a	0.00017	0.00026	Red clays
AM24 b		0.00008	Red clay, Neuquen sedimentary sequence
AM25	0.00357	0.00289	Lava masiva
AM26	0.00797	0.00491	Vesicular lava
AM27	0.00984	0.00833	Massive lava
AM28	0.01658	0.00829	Massive lava
AM29	0.02569	0.00897	Massive lava

computed the signature of a crustal slab with a constant magnetization of 2 A/m (Fig. 7) placed in a reverse polarity field. This value has been chosen on the basis of the range of the susceptibilities we got with the inversion algorithm. In a more general sense, an estimation of the terrain magnetic effect might be useful, either to identify sources related to the topography or to enhance the magnetic anomaly of buried sources obscured by the terrain effect. The upper surface of the slab coincides with the high-resolution Digital Elevation Model provided by YPF S.A., and the lower one is a surface standing at 500 m below the topographic elevation and following the trend of the latter. The chosen area is a 125 $\times$ 125 km square grid, whose center corresponds to the AM central edifice, covering the whole AM volcanic plateau and a wide area of the surroundings.

4.2. *Location and Depth of Magnetic Sources: The Euler Deconvolution*

In the last decades, several techniques were developed for locating magnetic contacts, and one of the most widely used is the Euler Deconvolution. This technique was originally presented by THOMPSON (1982); it consists in solving the Euleŕs homogeneity equation for different windows of data covering the whole magnetic anomaly map. The horizontal position and depth of the simple equivalent magnetic sources are obtained. To solve the equations, it is

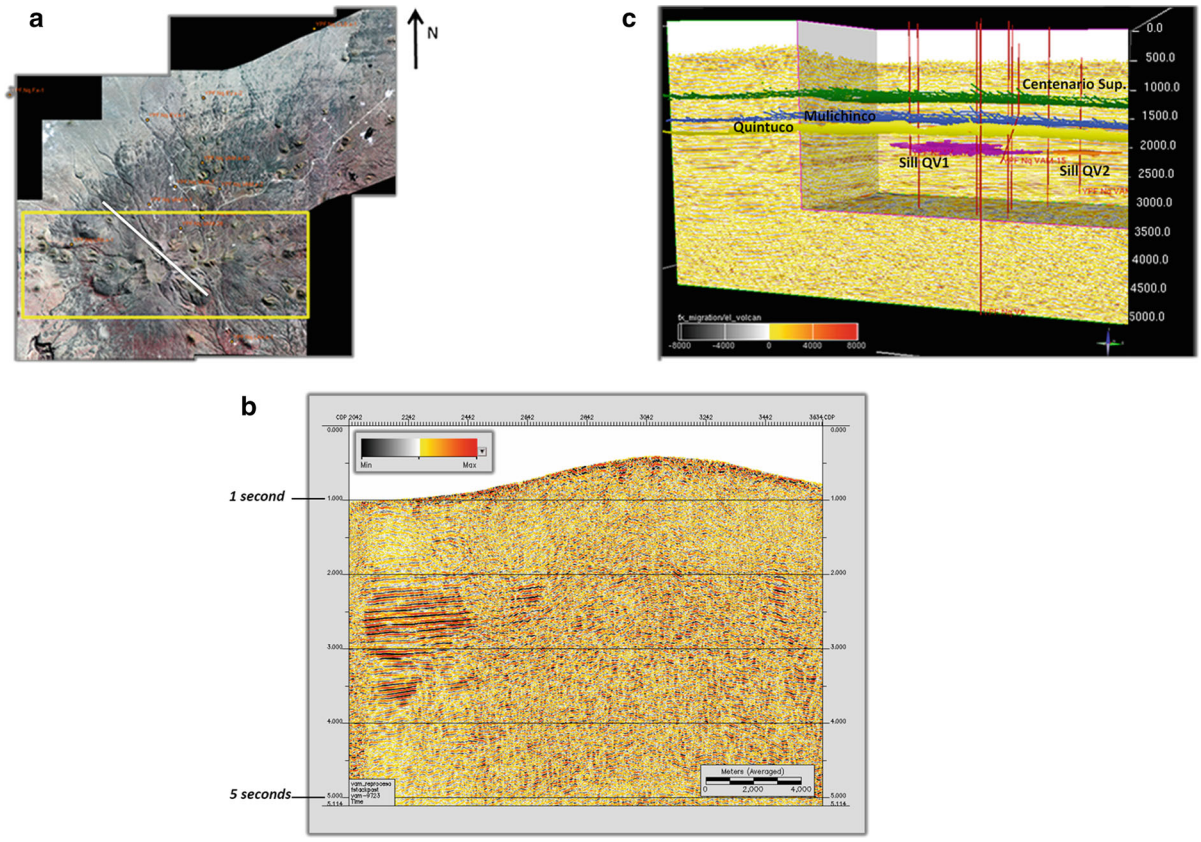

Figure 5

a Ikonos satellite image of the AM volcanic plateau. The *yellow rectangle* indicates the area with no 3D seismic data. **b** 2D NW–SE two ways travel time seismic section (*white line* in **a**) showing the low signal-to-noise ratio in the central crater area. Each subdivision in the vertical scale is a time interval of 1000 ms (1 s), **c** Main seismic horizons interpreted around the central crater (Mulichinco and Centenario Superior). QV1 and QV2 are two sills intruded in Quintuco-Vaca Muerta. *Vertical lines* are borehole trajectories. Planes are sections of the seismic cube. *Vertical axis scale* is time in milliseconds

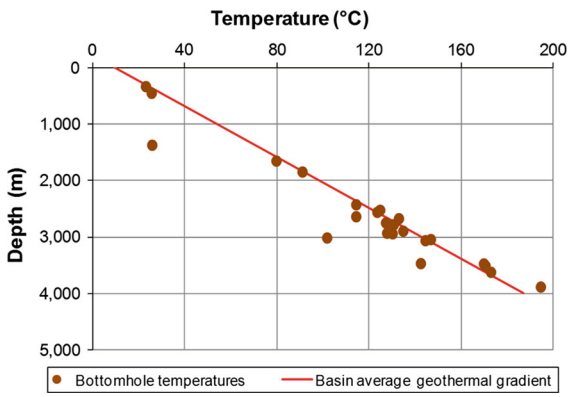

Figure 6

Subsurface temperature variation with depth. Points are temperature measurements in AM boreholes; the *solid line* corresponds to global average geothermal trend for the Neuquén Basin (Sigismondi and Ramos 2008)

necessary to assign a parameter, the structural index (SI), which is characteristic of each magnetic source. This index represents the rate of attenuation of magnetic anomaly with distance to the source. SI values vary between 0 and 3 depending on the geometry of the anomalous body. This method works well for simple sources, such as a magnetic dipole, line of dipoles, monopole, etc. Real sources, however, are not point sources but extended bodies equivalent to ensembles of dipoles. Reid *et al.* (1990), Barbosa *et al.* (1999, 2000), Mushayandebvu *et al.* (2001) and Hsu (2002), among others, also considered this method, with some variations. Model studies and theoretical work by Reid *et al.* (1990) have led to the conclusion that the location of magnetic sources of varying strikes in presence of a non-vertical field

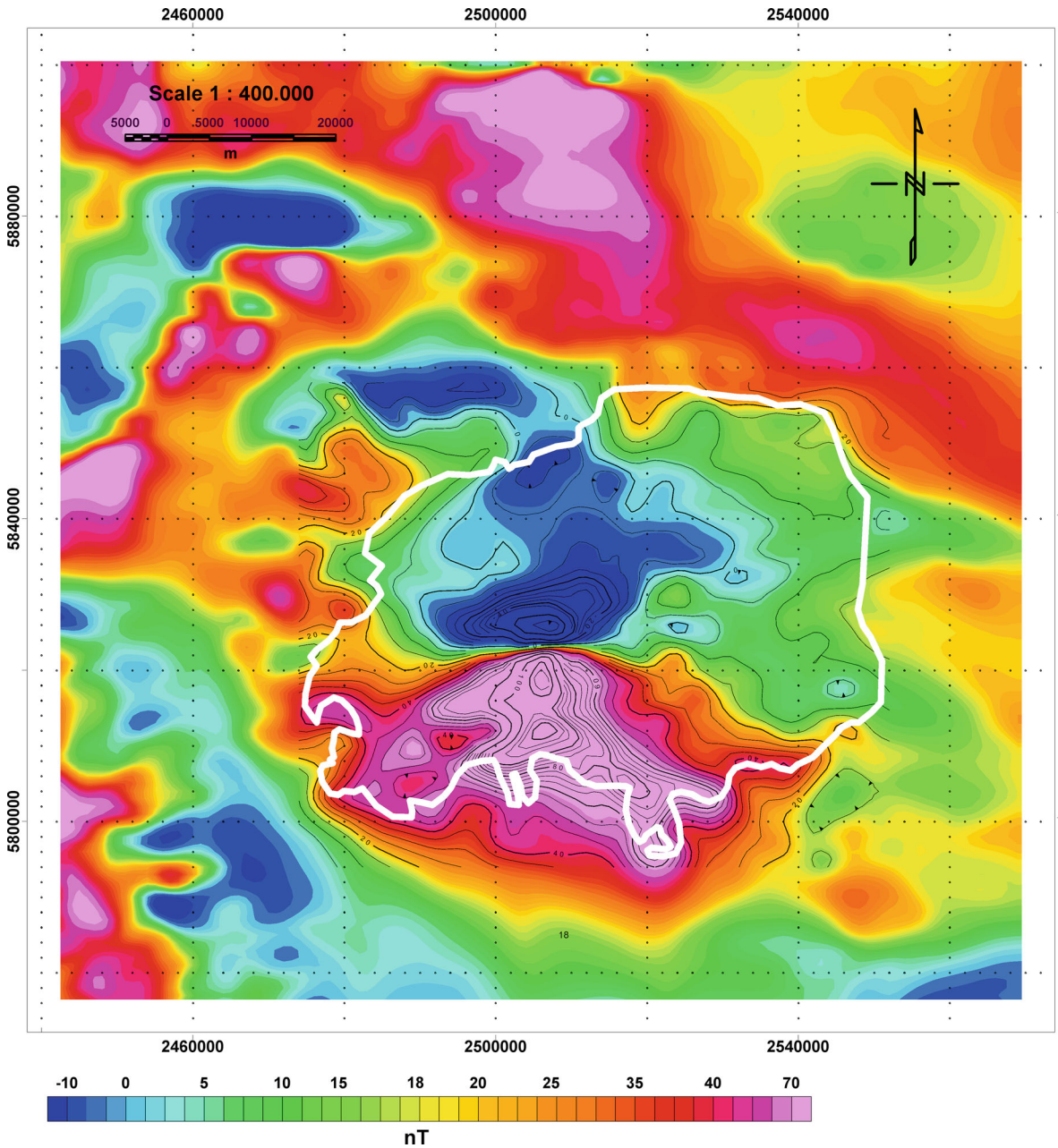

Figure 7
Computed topographic effect of a uniformly magnetized crustal slab placed in a reverse magnetizing field with $I = 57°$, $D = 142°$ and a constant magnetization of 2 A/m

can be accurately reproduced by Euler Deconvolution without applying Reduction-to-the-Pole. The method also yields useful results in the presence of remanence. No information on the dip of the sources is obtained; therefore, it must be estimated by other means, e.g., by inverse modeling.

The method was applied to the magnetic data of AM volcano using a 5 km window size and an SI

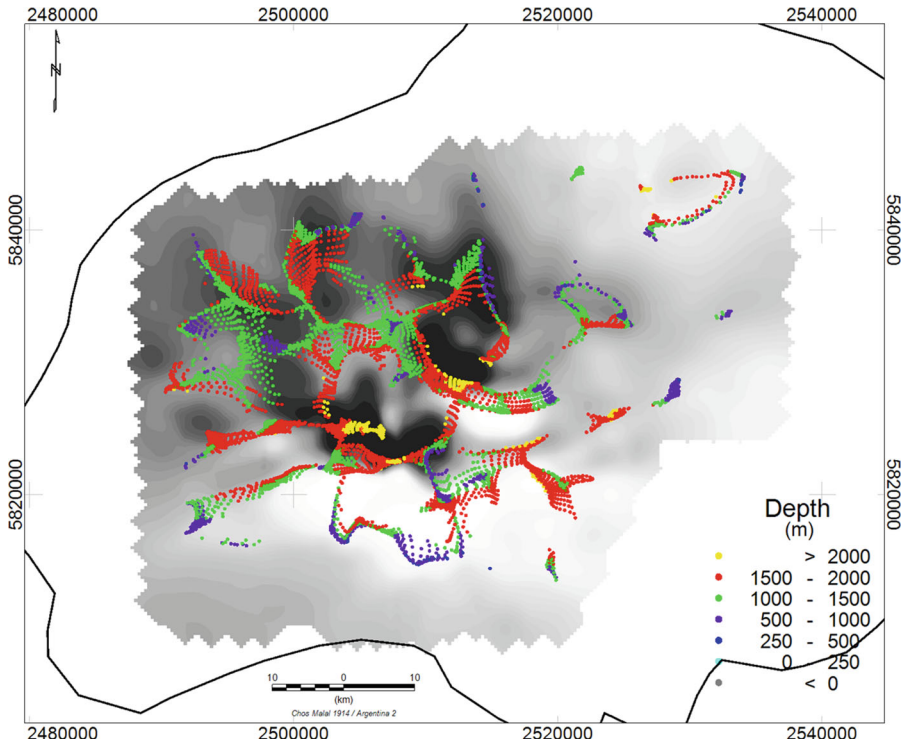

Figure 8
Euler Deconvolution solutions obtained from magnetic anomaly map with a window size of 5 km for SI = 1. The reference height is the sea level

equal to 1, corresponding to dikes or sills that are the most likely sources beneath the edifice. Figure 8 shows the Euler deconvolution solutions. Most of the solutions highlight sources mainly located at the anomaly boundaries, at depths between 1 and 2 km b.s.l., and other solutions deeper than 2 km b.s.l. The calculation was made such that only those solutions having a depth uncertainty less than 7 % were accepted. Horizontal location is correct within 15 % of the calculated depth.

4.3. *Spectral Analysis of the Magnetic Anomalies*

Fourier analysis represents a well-established procedure in potential field methods. It allows us to obtain information about the depth of the anomaly sources. Data spacing and the geographical extension of the survey poses some restrictions on the wavenumber and wavelength detectable by this analysis.

The AM magnetic anomaly field grid cell size (0.25 km x 0.25 km) and the area dimensions (35×40 km^2 approximately) determine the minimum and maximum wave number ($k_{\min}$, $k_{\max}$) of the recorded anomalies and the depth of the investigation limit. As a consequence, the anomaly map holds anomalies whose k values are between 2.6 10^{-2} and 2 km^{-1}. The maximum wavelengths are 35 and 40 km, whereas the Nyquist wavenumber is 0.5 km.

The depths to the top of the AM magnetic sources were obtained with the radially averaged power spectrum technique. While the energy spectrum is a 2D function of the energy relative to wavenumber and direction, the radially averaged energy spectrum (RAPS) is a function of wavenumber alone, and it is calculated by averaging the energy for all directions for the same wavenumber. The Fourier transform of the magnetic field produced by a prismatic body has a broad spectrum whose peak location is a function of the depth to the prisḿs top and bottom surfaces, and

whose magnitude is determined by the prisms magnetization. The peak wavenumber (k_{max}) can be determined by Eq. (1) (BLAKELY 1995):

$$k_{max} = \frac{\log\left(\frac{z_b}{z_t}\right)}{z_b - z_t}, \quad (1)$$

where z_t and z_b are the depths (measured from the flight elevation) to the top and bottom of the layer, respectively, k is the peak wavenumber in radians per unit of distance. When considering a grid large enough to include many sources, the log spectrum of the data can be interpreted to determine the statistical depth to the top. Therefore, depths are determined by measuring the slope of the energy power spectrum and dividing it by 4π (SPECTOR and GRANT 1970) as follows:

$$h = -s/4\pi, \quad (2)$$

where h is the depth and s is the slope of the log (energy) spectrum.

Figure 9 shows depth estimates based on 5-point averages of the slope of the energy spectrum of the AM volcano, giving a maximum depth of the ensemble of magnetic sources at about 3.5 km (below flight elevation).

4.4. Reduction-to-the-Pole

Reduction-to-the-Pole (RTP) is one of the most widely used algorithms in magnetic data processing. It consists of generating the magnetic anomaly field that would be recorded, if the source bodies were placed at the earth's magnetic poles. Therefore, the effects associated with the inclination of the field with latitude are removed and each dipolar anomaly is transformed into positive or negative counterparts located directly above the source facilitating its interpretation. The algorithm approximates the ambient magnetic field and the rock magnetization to constant average values (amplitudes and directions) for the entire study region. This is a reasonable assumption provided that the area of investigation has a limited geographical extension. An accurate RTP transformation in the presence of strong remanence requires both induction and remanent magnetization components. The AM volcanic activity developed during the Pliocene and Pleistocene times; in this time span the Earth's magnetic field reversed several times. In the previous sections, we argued that AM magnetic anomaly field shows prevailing reverse magnetized sources. Therefore, most of the magnetized sources emplaced in a reverse chron and the remanence is the dominant magnetization component of the AM rocks. Consequently, meaningful values for these parameters have to be selected in order to carry out the RTP transformation. Remanence values are chosen in agreement with previous paleomagnetic studies for the study area (Propiedades magnéticas de los basaltos del área del Auca Mahuida, Laboratorio de Paleomagnetismo 'Daniel Valencio', Universidad de Buenos Aires, unpublished data). Thus, we computed the Reduced-to-the-Pole field for two separate cases, one considering the source magnetization as due to induction alone (with angular values $I = -38°$ and $D = 3°$, Fig. 10a), and the other one as due to induction and remanence (Fig. 10b). As discussed above, the latter was considered to be acquired in an inverse chron with average inclination and declination of 38° and −177°, respectively.

4.5. Analytic Signal

The analytic signal (AS) method was introduced by NABIGHIAN (1972, 1984). It represents the energy envelope of the magnetic anomalies, and its amplitude $A(x, y)$ is a function of the orthogonal gradients of the anomalies (ROEST *et al.* 1992):

$$|A(x,y)| = \left[(\partial T/\partial x)^2 + (\partial T/\partial y)^2 + (\partial T/\partial z)^2\right]^{1/2}, \quad (3)$$

where T is the total magnetic intensity anomaly. The AS is independent of the direction of magnetization and of the Earth's magnetic field. This characteristic is particularly advantageous where strong remanence is present, or at low magnetic latitude. In fact, MACLEOD *et al.* (1993) proposed that AS is an alternative to Reduction-to-the-Pole for low latitudes. Independence of magnetization direction means that all bodies with the same geometry have the same analytic signal. Furthermore, as the peaks of analytic signal functions are symmetric and occur directly over the edges of wide bodies and over the centers of narrows bodies, the interpretation of analytic signal

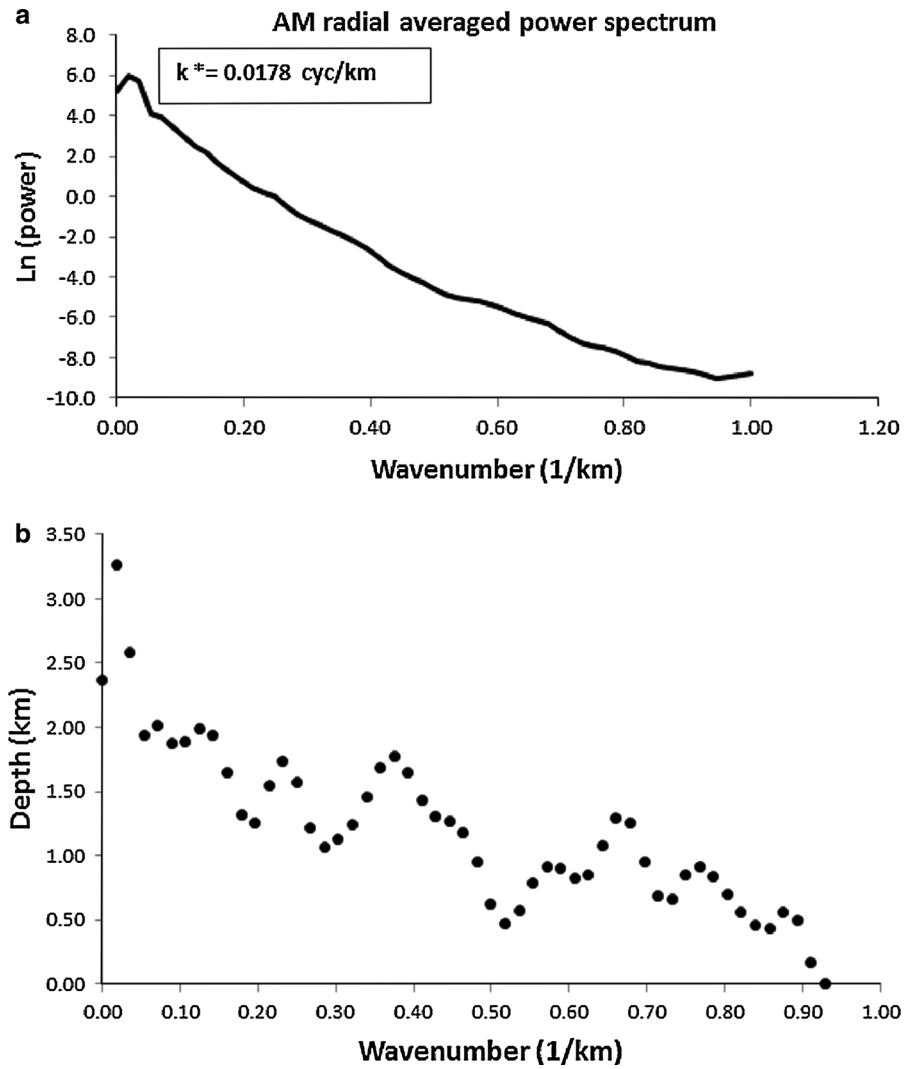

Figure 9

a Depth estimation of magnetic sources from radially averaged logarithmic energy spectrum of the AM anomaly field. The spectrum corresponds to ensembles of magnetic bodies with the same average depth; k^* is the wavenumber value for the maximum of the power spectrum. **b** Depth estimates from the slopes of the spectrum taken in 5-point intervals

maps should provide indications of magnetic source geometry (Gunn 1997). Nabighian (1972) showed that the maxima of AS are located over the magnetization contrasts, so they can be used to indentify the main contrasts.

Nabighian (1972) used the AS amplitude to estimate the depth to the magnetic contact. Roest *et al.* (1992) and Atchuta Rao *et al.* (1981) used the anomaly width at half the amplitude to derive the depths. However, the measured amplitude is usually due to many overlapping anomalies and, even when the amplitude can be well determined for a single source, the resulting depth will be not well constrained if the correct model is not used. For the above mentioned reasons, we do not use this technique to estimate depths since the TMI anomaly map at AM volcano is produced by an ensemble of small anomalies.

In order to determine the main magnetization contrast of the TMI map, we calculate the AS

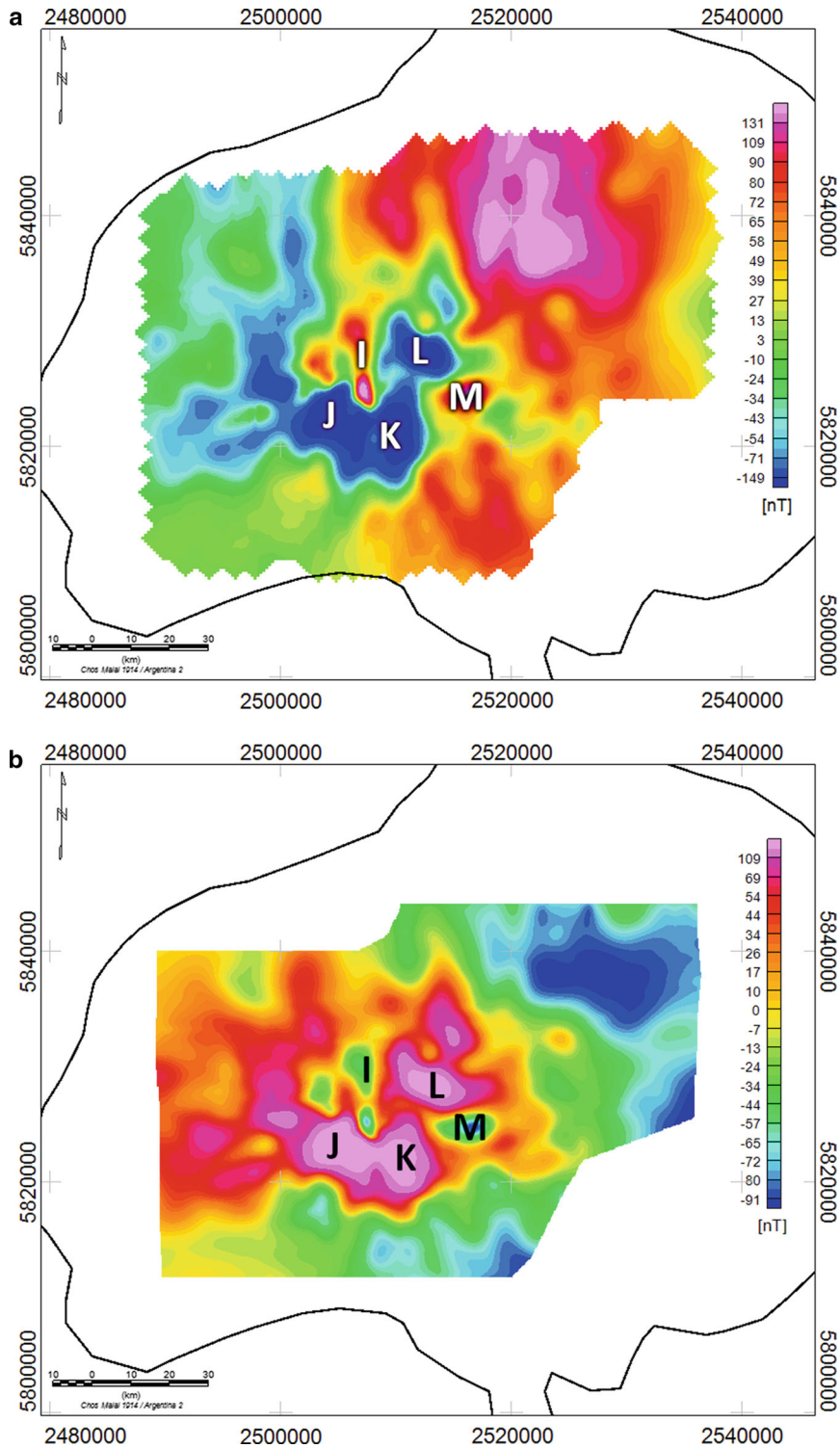

Figure 10
a RTP transform computed considering only the induction component ($I = -38°$ and $D = 3°$). **b** RPT transform computed with both induced and remanent magnetizations ($I = 38°$ and $D = -177°$). The anomalies are labeled with *black letters* (see Fig. 3 for comparison)

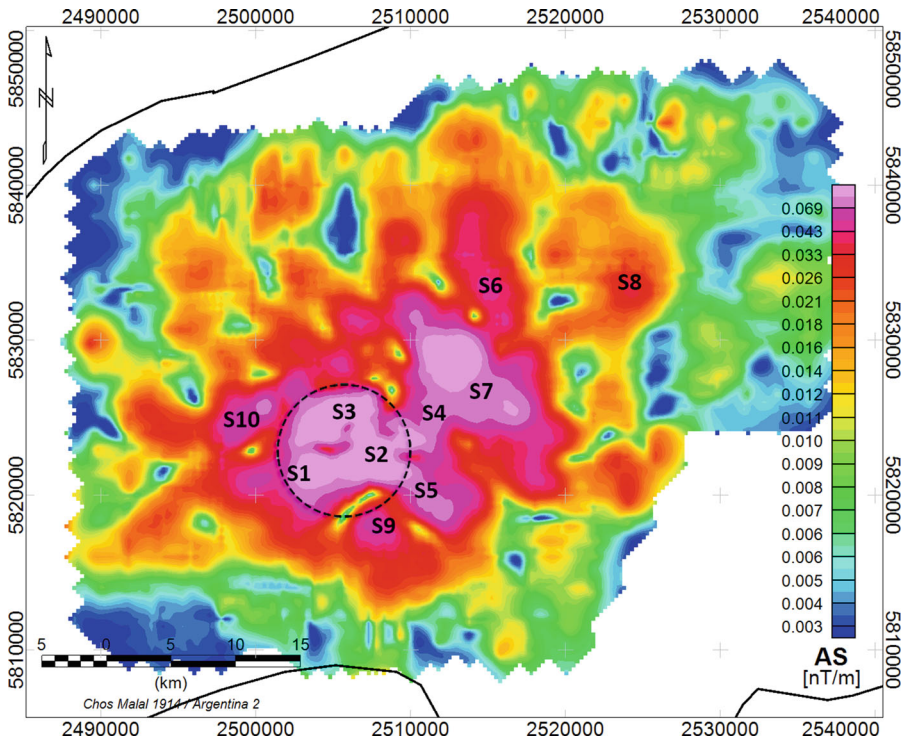

Figure 11
Amplitude map of the analytic signal obtained from TMI anomaly. The *dashed circle* indicates the central crater of the volcano. S1 to S10 are the main sources causing the amplitude peaks. Units of AS amplitude are [nT/M]

amplitude (Fig. 11). Its shape is similar to that of the Reduced-to-the Poles transform anomaly with remanence effect (Fig. 10b).

5. *Inverse modeling*

In most of the inversion methods, it is assumed that the magnetic response arises from induced magnetization. When this is true, reliable results can be obtained. However, if the remanence is important, more realistic results will be obtained by modeling the magnetization as a vector. This is because remanent magnetization can distort inversions based on the assumption that the source has only induced magnetization (MacLeod 2013). The magnetic vector inversion (MVI) makes use of both the induced and remanent magnetization without a priori knowledge of the direction of the latter. MVI allows to change the direction of magnetization inside the model and thus it takes into account the combined effects of remanence and induced magnetization. The result is a more realistic representation of the rock magnetization. On the contrary, conventional susceptibility inversion is based on the premise that the magnetic domains in all rocks orient themselves parallel to the geomagnetic field. This results in negative susceptibility values, which are artifacts of the calculation, since a negative susceptibility is physically unreasonable.

The MVI technique was applied to the AM volcano data to obtain a magnetization cube using VOXI Earth Modeling from GeosoftTM. Elevation in the model ranges between 2175 and −5038 m (with z values positive above the sea level). The grid constructed to process the data has a cell size of 500 m in the x and y directions, and a vertical size of 465 m in the z direction. Figure 12a shows the isosurface of 0.012 SI from the magnetic vector inversion (light blue shapes surrounding the central areas) together with the topography grid. The highest susceptibility values we got are about 0.13 SI; Fig. 12b is a plot of

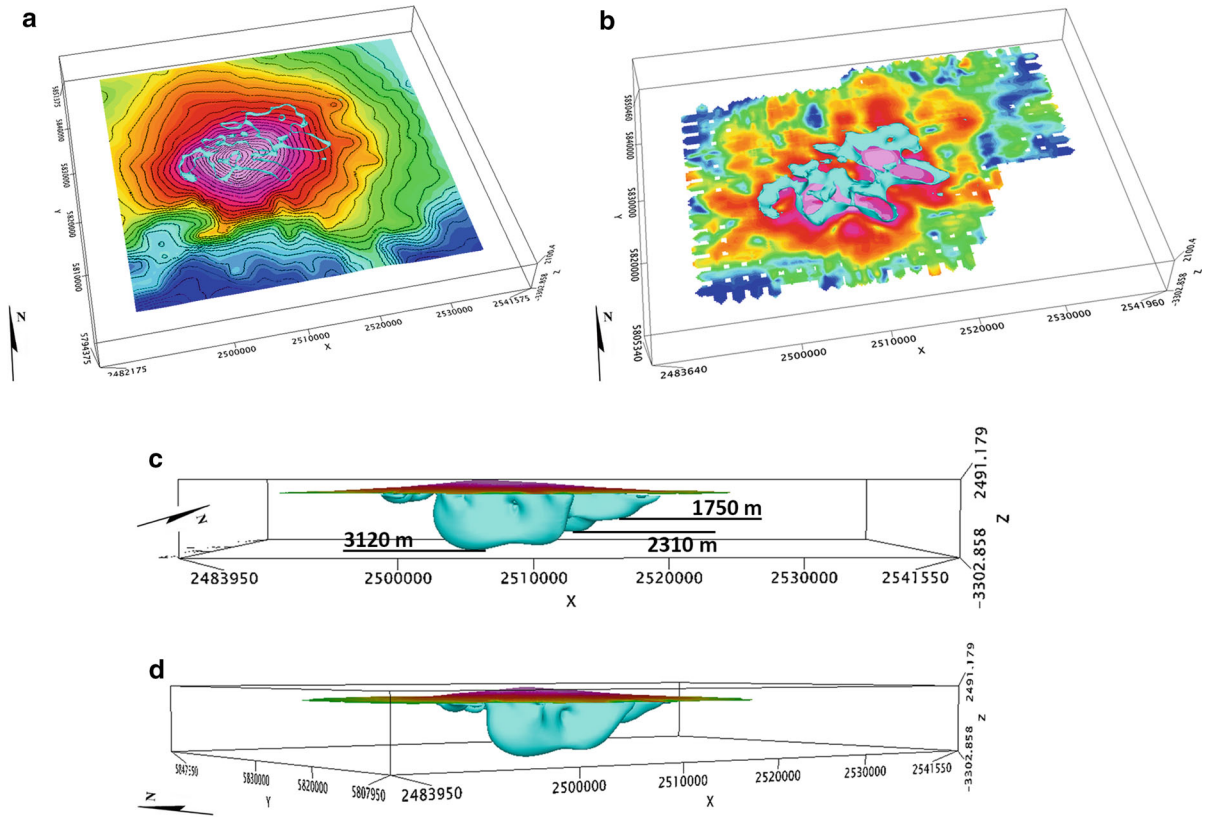

Figure 12
a 3D representation of the magnetic vector inversion results, the 0.012 SI isosurface roughly represents the magnetic anomalies source bodies (*light blue shapes* surrounding the central areas) along with the topography layer. **b** The 0.012 SI isosurface plot along with the analytic signal **c**, **d** Different views of the 0.012 SI isosurface near the central crater. The *color surface on top* is the topography. *Z* direction is positive above sea level

the analytic signal derived from the AM TMI anomaly data, together with the same 0.012 SI isosurface. It can be seen that there is a good correspondence between the source locations and the analytic signal map. A similar behavior was observed in other studies, and it was interpreted as having geological consistency (MacLeod 2013). Finally, panels (c) and (d) of Fig. 12 show two views of an E-W section of the 0.012 SI isosurface, where the depth extent of the bodies reaches about 3 km b.s. l.

6. *Discussion and Conclusions*

The magnetic anomaly map of the Auca Mahuida volcano (Fig. 3) shows an ensemble of sources with a prevailing reverse magnetization. The age of the AM rocks (Ramos and Folguera 2010) suggest that most of the sources emplaced during the reverse polarity Matuyama Chron. AM anomalies lie around the central crater with wavelengths between 1.5 and 5 km. These anomalies do not correlate with any topographic effect shown on Fig. 7, confirming their deep origin. The maximum subsurface temperatures, recorded at approximately 4 km b.s.l., are about 180 °C, a value lower than the Curie temperature, as previously reported. Thus, the igneous bodies intruded into the sedimentary sequence of the Neuquén basin are not thermally demagnetized.

The Reduced-to-the-Pole field computed considering only the induction component of the magnetization shows that the algorithm is not able to correctly transform the normally magnetized anomalies (such as the features I and M of Fig. 3 and

10a) since they do not change their positions. Instead, the anomalies J, K, and L are shifted above their source, but they are transformed in negative monopolar features (therefore changing their sign with respect to the TMI field). This implies that TMI is affected by inverse remanence since the algorithm verticalizes the anomaly axis along the present Earth field direction, which is opposite to that along which the sources bodies were magnetized. The Reduced-to-the-Pole field computed considering both the induction and remanence shows that the transformation does not remove the dipolar feature either, but the anomalies polarity is exactly opposite to that of the field of Fig. 10b. Therefore, the RTP fields obtained with and without remanence are very similar, but with opposite sign. In fact, the remanence relates to a reverse field that simply inverts the polarity and does not change considerably the configuration of the magnetic pattern.

The analytic signal maxima highlight peaks of the magnetization around the AM central crater (S1, S2, S3 in Fig. 11), as well as in the eastern sector, where NW–SE oriented (S4, S5, S7) high and lower intensity features (S6 and S8) are observed. This preferential direction coincides with the strike of the Entre Lomas fault system and with the axis of the anticline over which AM emplaced.

The magnetic field spectral analysis indentifies sources at shallow depth with a maximum of 3.5–4 km below flight elevation. Besides, most of the Euler Deconvolution solutions highlight depths around 1 km and 2 km b.s.l, and few others deeper than 2 km. These results are consistent with the depth of the bodies obtained using the MVI inversion modeling (Fig. 12) clustered in the central zone and elongated mainly in NW–SE direction. This orientation indicates that the shallow intrusive structures of the volcano are controlled by the NW–SE striking Entre Lomas faults (Late Jurassic to Upper Cretaceous periods), which affects the basement below the eastern sector of the volcanic edifice. The sub-volcanic bodies represent the crystallized dikes and sills mainly intruded in the Quintuco - Vaca Muerta and Mulichinco Formations, and the Cuyo Group. Their geometry is consistent with that inferred from seismic and well data (Fig. 5c). The magma upraised through previously existing faults and contributed to their sealing; as a consequence, the properties of the surrounding rocks were altered. The fracturing due to the differential heating and cooling of the intrusions and of the surrounding rocks increased the local porosity and permeability giving rise to different rock qualities in the hydrocarbon reservoir. Moreover, volcanism likely contributed to the thermal hydrocarbon generation (Pángaro *et al*. 2004; Vottero *et al*. 2005). In fact, the organic matter coalification was speeded by higher temperatures and in some cases oil prematurely migrated from the source rocks (e.g., Vaca Muerta) along pre-existing fractures and was trapped in the fractured intrusions. The higher magnetization of these volcanics in comparison with the surrounding non-magnetic sedimentary layers allows the detectability of potential oil traps through the magnetic prospecting. As a consequence, intrusive position, depths, geometry, and volume provided by the magnetic modeling are valuable information.

The analysis of the magnetic anomaly field has provided information on the shallow structure of the AM feeding system. The NW–SE and E–W strikes of the modeled sources agree with those of the regional fault systems proving their key role in the control of the AM volcanism. These results point out the effectiveness of the magnetic prospecting methods in presence of strong remanent magnetization.

Acknowledgments

We are grateful to YPF S.A. Company for providing the data used in this study and the permission to publish. We also thank Telma Aisengart of Geosoft for the support to build the inverse model and Hernán Scuka of YPF for the valuable help to improve the quality of the figures. We also acknowledge the two anonymous reviewers for their efforts to improve the quality of the work and the Editor William L. Bandy for the handling of the manuscript.

References

Atchuta Rao, D., Ram Babu, H.V., and Sanker Narayan, P.V., 1981, *Interpretation of magnetic anomalies due to dikes: the complex gradient method*. Geophysics, 46, 1572–1578.

Barbosa V., Silva J. and Mediros, W., 1999, *Stability analysis improvement of structural index estimation in Euler Deconvolution*. Geophysics, 64, 48–60.

Barbosa V., Silva J. and Mediros, W., 2000, *Making Euler Deconvolution applicable to small ground magnetic surveys*. Journal of Applied Geophysics, 43, 55–68.

Blakely, R.J., and Grauch, V.J.S., 1983. *Magnetic models of crystalline terrane: accounting for the effect of topography*. Geophysics, 48, 1551–1557.

Blanco-Montenegro I., l Torta J. M., García A., Araña V., 2003, *Analysis and modeling of the aeromagnetic anomalies of Gran Canaria (Canary Islands)*. Earth and PlanetaryScienceLetters, 206, 601–616.

Blanco-Montenegro, I., De Ritis, R., & Chiappini M., 2006. *Imaging and modeling the subsurface structure of volcanic calderas with high-resolution aeromagnetic data at Vulcano (Aeolian islands, Italy)*, B. Volcanol., 69 (6), p. 643–659, doi:10.1007/s00445-006-0100-7.

Bermúdez, A., Delpino, D., 1998, Estudio de testigos corona de rocas ígneas intrusivas reservorios de hidrocarburos y de las secuencias del Volcán Auca Mahuida. Repsol YPF. Unpublished report.

Blakely, R. J. Potential Theory in Gravity and Magnetic Applications (Cambridge University Press, New York, 1995)

Brisson, I., and Veiga, V., 1999, YPF internal report.

Carson Aereogravity, 2001,VolcánAucaMahuida and Señal Cerro Bayo Exploration Lots (March 28, 2001 - June 10, 2001). For YPF S.A., Argentina. Data Processing Report.

Cristallini, E.O., Bottesi, G., Gavarrino, A., Rodriguez, L., Tomezzoli, R., Comeron, R., 2006, Synrift geometry of the Neuquén Basin in the northeastern Neuquén Province, Argentina, InEvolution of the Andean margin: a tectonic and magmatic view from the Andes to the Neuquén Basin (35 –39 422 latitude): Geological Society of America. eds. Kay, S. M. and Ramos, V. A.). Special Paper 407, pp. 147–161.

De Ritis, R., Blanco-Montenegro, I., Ventura, G., Chiappini, M., 2005, Aeromagnetic data provide new insights on the volcanism and tectonics of Vulcano Island and offshore (Southern Tyrrhenian Sea, Italy), Geophysical Research Letters, 32, L15305, doi:10.1029/2005GL023465.

Finn, C., Sisson, T. W. & Deszcz-Pan, M., 2001. *Aerogeophysical measurements of collapse-phrone hydrothermally altered zones at Mount Rainer volcano*, Nature, 409, 600–603.

Gunn P.J., 1997, *Quantitative methods for interpreting aeromagnetic data: a subjective review*. AGSO Journal of Australian Geology & Geophysics, 17(2), 105–113.

Hsu, S., 2002, *Imaging magnetic sources using Euleŕs equation*. Geophysical Prospecting, 50, 15–25.

Kay, S.M., and Ramos, V.A., 2006, Evolution of an Andean Margin: A tectonic and magmatic view from the Andes to the Neuquén Basin (35°–39°S): Geological Society of America, Special Papers, v. 407, 19–60, 10.1130/2006.2407(02).

Longo, L.M., Ravazzoli, C.L.,Chiappini, M., 2008, Proyecto de interpretación de datos aerogravimétricos y magnéticos en el Volcán Auca Mahuida. Cuarto encuentro ciéntifico del ICES (E-ICES4), Malargüe, Mendoza, Argentina.

MacLeod, I.N, Jones, K., Fan Dai, D., 1993, 3-D analytic signal in the interpretation of total magnetic field data at low magnetic latitudes. Explor. Geophys., 24, 679-688.

MacLeod, I.N., Ellis, R.G., Magnetic Vector Inversion, a simple approach to challenge of varying direction of rock magnetization.23 rd International Geophysical conference and exhibition, 11–14 August 2013. ASEG-PESA 2013Melbourne, Australia.

Mosquera, A. and Ramos, V.A., 2006, Intraplate deformation in the Neuquén Basin, In: Kay S.M. and Ramos, V.A., eds. Evolution of an Andean margin: a tectonic and magmatic view from the Andes to the Neuquén Basin (35 –39 S latitude). Geological Society of America Special Paper, 407, 97–124.

Mushayandebvu, M.,Van Driel, P., Reid, A. and Fairhead, J., 2001, *Magnetic source parameters of two-dimensional structures using extended Euler Deconvolution*. Geophysics, 66, 814-823.

Nabighian, N.M., 1972, *The analytic signal of two-dimensional magnetic bodies with polygonal cross section: its properties and used for automated anomaly interpretation*. Geophysics 37, 507-517.

Nabighian, N.M., 1984, *Toward a three-dimensional automatic interpretation of potential field data* via *generalized Hilbert transforms: fundamental relations*, Geophysics 49, 780-786.

Pángaro, F., Villar, H., Vottero, A., Bojarski, G., Rodríguez Arias, L., 2004, Eventos volcánicos y sistemas petroleros: El caso del Volcán Auca Mahuida, Cuenca Neuquina, Argentina. IX Congreso Latino americano de Geoquímica orgánica, México, 23-27.

Ramos, V.A. and Folguera, A., 2010, Payenia volcanic province in the Southern Andes: an appraisal of an exceptional Quaternary tectonic setting: Journal of Volcanology and Geothermal Research, v. 201, 53–64, doi:10.1016/j.jvolgeores.2010.09.008.

Reid, A., Allsop, J. Granser, H., Millet, A. and Somerton, I., 1990, *Magnetic interpretation in three dimensions using Euler Deconvolution*. Geophysics, 55, 80-91.

Reynolds J. M., An Introduction to Applied and Environmental Geophysics (John Wiley & Sons, 2011-2nd Edition)

Roest, W.R Verhoeff, J. Pilkington, M., 1992. *Magnetic interpretation using the 3-D analytic signal*. Geophysics 57, 116–125.

Rossello, E.A., Cobbold, P.R., Diraison, M., and Arnaud. N., 2002, Aucamahuida (Neuquén basin, Argentina): A Quaternary shield volcano on a hydrocarbon-producing substrate, in 6th International Symposium on Andean Geodynamics (ISAG 2002). Extended Abstracts, Barcelona, Univ. De Barcelona: Instituto Geologico y Minero de España, 549–552.

Sigismondi, M. and Ramos, V., 2008,El flujo de calor de la cuenca Neuquina, Argentina. VII Congreso Exploración y Desarrollo (Simposio de La Geofísica: Integradora del conocimiento del subsuelo).

Spector, A. and Grant, F.S., 1970, *Statistical models for interpreting aeromagnetic data*, Geophysics, 35, 293–302.

Thompson, D., 1982, EULDPH: *A new technique for making computer-assisted depth estimates form magnetic data*. Geophysics, 47, 31–37.

Vela R., Sancho V., Fasola M., 2006, Integración de datos geoquímicos en el desarrollo del yacimiento volcán Auca Mahuida. III Workshop de Geoquimica de Sistemas Petroleros, Quito, Ecuador, Abril 2006.

VENTURA, G., DE RITIS, R., LONGO, M., CHIAPPINI, M., 2012, *Terrain characterization and structural control of the Auca Mahuida volcanism (Neuquén Basin, Argentina)*: International Journal of Geographical Information Science, v. 27, 1469-1480, doi:10.1080/13658816.2012.741241.

VOTTERO, A., RODRÍGUEZ, L., VELA, R., 2005, Trampas de hidrocarburos en el centro este de la Cuenca Neuquina. VI Congreso de Exploración y Desarrollo de Hidrocarburos- Las trampas de hidrocarburos en las cuencas productivas de Argentina, 189–208.

(Received May 4, 2015, revised July 31, 2015, accepted August 1, 2015, Published online August 14, 2015)